Integrative Biology

RSC Publishing

PAPER

View Article Online
View Journal | View Issue

Cite this: *Integr. Biol.*, 2013, **5**, 569

Hutchinson–Gilford progeria syndrome alters nuclear shape and reduces cell motility in three dimensional model substrates†

Elizabeth A. Booth-Gauthier,[a] Vicard Du,[b] Marion Ghibaudo,[b] Andrew D. Rape,[c] Kris Noel Dahl*[ac] and Benoit Ladoux*[bd]

Cell migration through tight interstitial spaces in three dimensional (3D) environments impacts development, wound healing and cancer metastasis and is altered by the aging process. The stiffness of the extracellular matrix (ECM) increases with aging and affects the cells and cytoskeletal processes involved in cell migration. However, the nucleus, which is the largest and densest organelle, has not been widely studied during cell migration through the ECM. Additionally, the nucleus is stiffened during the aging process through the accumulation of a mutant nucleoskeleton protein lamin A, progerin. By using microfabricated substrates to mimic the confined environment of surrounding tissues, we characterized nuclear movements and deformation during cell migration into micropillars where interspacing can be tuned to vary nuclear confinement. Cell motility decreased with decreased micropillar (μP) spacing and correlated with increased dysmorphic shapes of nuclei. We examined the effects of increased nuclear stiffness which correlates with cellular aging by studying Hutchinson–Gilford progeria syndrome cells which are known to accumulate progerin. With the expression of progerin, cells showed a threshold response to decreased μP spacing. Cells became trapped in the close spacing, possibly from visible micro-defects in the nucleoskeleton induced by cell crawling through the μP and from reduced force generation, measured independently. We suggest that ECM changes during aging could be compounded by the increasing stiffness of the nucleus and thus changes in cell migration through 3D tissues.

Received 28th September 2012,
Accepted 19th January 2013

DOI: 10.1039/c3ib20231c

www.rsc.org/ibiology

Insight, innovation, integration

The premature aging disorder Hutchinson–Gilford progeria syndrome is associated with the expression of the mutant nucleoskeletal protein progerin. Despite significant molecular understanding of the disorder, it is unclear how the expression of a mutant protein leads to a systemic aging pathology. Using engineered 2D and 3D extracellular matrices, we quantify cellular force generation and motility through tight interstitial spaces. Progeriod cells show increased nuclear defects, reduced force generation and decreased nuclear deformability, which both lead to reduced cellular motility. Decreased cell motility in tight interstitia could have an impact on wound healing, development and other biomechanical processes.

Introduction

Cell migration through tight interstitia is important in many physiological and pathological processes including development, wound healing, inflammation, and tumor cell metastasis. Generally, tissue regeneration in native or artificial matrices requires cellular invasion and transmigration through tight structures.[1,2] As cells migrate through 3D tissues, they can encounter a broad range of mechanical cues including various stiffnesses and topographic features of the surrounding extracellular matrix (ECM). Moving the cell body forward thus represents a physical challenge.[3] To overcome such mechanical constraints,

[a] *Department of Chemical Engineering, Carnegie Mellon University, 5000 Forbes Ave, Pittsburgh, PA 15213, USA. E-mail: krisdahl@cmu.edu*
[b] *Laboratoire Matière et Systèmes Complexes, Université Paris Diderot and Centre National de la Recherche Scientifique UMR 7057, Batiment Condorcet, 10 rue Alice Domon et Léonie Duquet, F-75205 Paris cedex 13, France. E-mail: benoit.ladoux@univ-paris-diderot.fr*
[c] *Department of Biomedical Engineering, Carnegie Mellon University, 5000 Forbes Ave, Pittsburgh, PA 15213, USA*
[d] *Mechanobiology Institute (MBI), National University of Singapore, 5A, Engineering Drive 1, Singapore 117411*

† Electronic supplementary information (ESI) available: Electronic supplementary movies are captions are provided online. See DOI: 10.1039/c3ib20231c

cells can degrade the ECM through proteolytic activity and must still undergo large deformations of their body to fit through the available space.[4] Traditional research of cell invasion and transmigration in microenvironments thus investigates focal adhesions, cytoskeleton, acto-myosin force generation, and proteolytic cleavage of the ECM, as well as chemical and mechanical signals from the ECM.[3,5–8] These studies of invasion focus on cellular driving forces, but there is a significant resistance to cellular invasion from subcellular structures. The nucleus is the largest and densest organelle in most cells and may be responsible for restricting cell invasion through extracellular matrices.[4,9] Furthermore, increasing evidence shows that cytoplasmic structures such as the actin cytoskeleton apply forces to modulate nuclear shape through nuclear-anchoring structures.[10,11]

The nucleus contains the genomic DNA and the stiff nucleoskeletal network at the inner nuclear membrane.[12] The nucleoskeleton consists of type V intermediate filaments formed from lamins. Lamin A is suggested to be responsible for the stiffness of the nucleoskeleton.[4] Many mutations are found in lamin A including mutations that cause Hutchinson–Gilford progeria syndrome (HGPS), a premature aging disorder.[13] HGPS patient cells have nuclei with a thickened nucleoskeleton, altered heterochromatin organization, and dysmorphic shape.[14,15] HGPS patient cells and cells that exogenously express progerin have stiffened nuclei,[16] and these cells do not properly respond to extracellular forces.[17]

Progerin accumulates quickly in patients with HGPS and is also sporadically produced during normal aging.[18] Generally, the nucleus acquires defects during aging.[19] It appears that many aspects of the body stiffen with aging: from the extracellular matrix outside the cell[20,21] to the nucleus within the cell.[20] The increased stiffness of the nucleus in an aged population could inhibit migration of cells throughout the body, slow recovery from injury, and limit cell invasion and transmigration into biomaterial implants. To test this concept, we used microfabrication techniques[22] to mimic 3D matrices[8,23,24] and control cell confinement under well-defined conditions.[22] We studied fibroblasts from an HGPS patient and a healthy adult control in three-dimensional (3D) microfabricated environments composed of uniformly spaced pillars whose interpillar spacing can be easily tuned to vary cell–matrix interactions. Cells were monitored as they moved from a flat substrate into a pillared substrate with interpillar spacing of 6, 8 and 12 μm. Normal cell nuclei were able to easily enter and exit the micropillar (μP) array and were able to quickly adapt and change shape. Tight μP spacing caused increased nuclear defects in HGPS patient cells, and fewer cells were able to enter the μP array than in the normal cells. Cells from HGPS patients and cells overexpressing progerin showed that, with accumulated defects in the nucleoskeleton, there was a decreased ability to move through the μPs. HGPS cells also showed reduced traction force in 2D, suggesting both reduced force generation and increased resistance may impact invasion and transmigration of aged cells.

Results

Nuclear morphology and lamin structure inside 3D micropillar array

To measure how nuclear deformability impacts cell movement through a tight ECM, we developed a physical ECM mimic using μP. We used polydimethylsiloxane (PDMS) μP arrays, originally developed to measure traction forces,[25,26] that are 20 μm high and completely coated in fibronectin. The height of the μPs reduced cellular migration over pillars and encouraged migration through the μP array.[22,27] The dimensions and spacing of the μP in the array were chosen to constrict and deform the nucleus as the cell moves within the μP. Here, diameter of the μP and spacing between the edges of individual μP will be denoted as diameter–spacing (D–S in μm). As a comparison, nuclei in cells were also observed in the 2D culture next to the μP array ('flat').

Quantifying nuclear shape in the μP array provides information about how adaptive the nuclei are to 3D structures. On flat substrates HGPS patient cells had dysmorphic nuclei with blebbing, invaginations, and creasing, compared with the ovoid control nuclei (Fig. 1 and 2).[28] Fig. 1 shows examples of invaginations, creases, and blebbing; nuclei are counted as dysmorphic with the presence of at least one of these features. Both control and HGPS fibroblasts inside the μP array show altered nuclear shapes with decreased pillar spacing (Fig. 1). Most HGPS cell nuclei were dysmorphic both on flat substrates and inside the μP array, Fig. 1D. Control cells show mostly smooth, ovoid nuclei on the flat substrate becoming deformed but smooth within the μP array. In the μP array, both HGPS and control fibroblasts show actin cytoskeleton extensions between the μP (Fig. 2), suggesting that cells were only able to move in between the μP and not over the top of the array.

A majority of the dysmorphic characteristics (Fig. 1) reflected nucleoskeletal changes including folds and micro-invaginations. We also quantified gross nuclear parameters including whole-nucleus size and shape (Fig. 3). Control cells

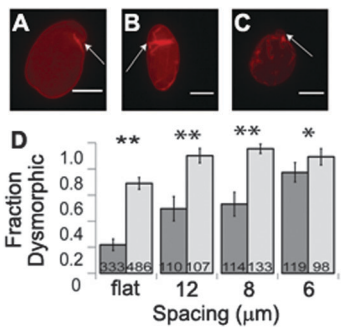

Fig. 1 Nuclear dysmorphisms characteristic of HGPS. Images of immunostained lamin A/C with Alexa Fluor 555 highlighting dysmorphic characteristics including invaginations (A), creasing (B), and blebbing (C). (D) Fraction of cells that displayed one or more of the dysmorphic phenotypes for varied pillar spacing. Fisher's exact test was used to compare between control (dark gray) and HGPS (light gray) populations. Numbers at the bottom of bar graphs are counts of cells used in analysis. Spacing numbers refer to diameter–spacing (D–S). Error bars are 95% confidence intervals with $*p < 0.05$, $**p < 0.01$. Scale bars are 10 μm.

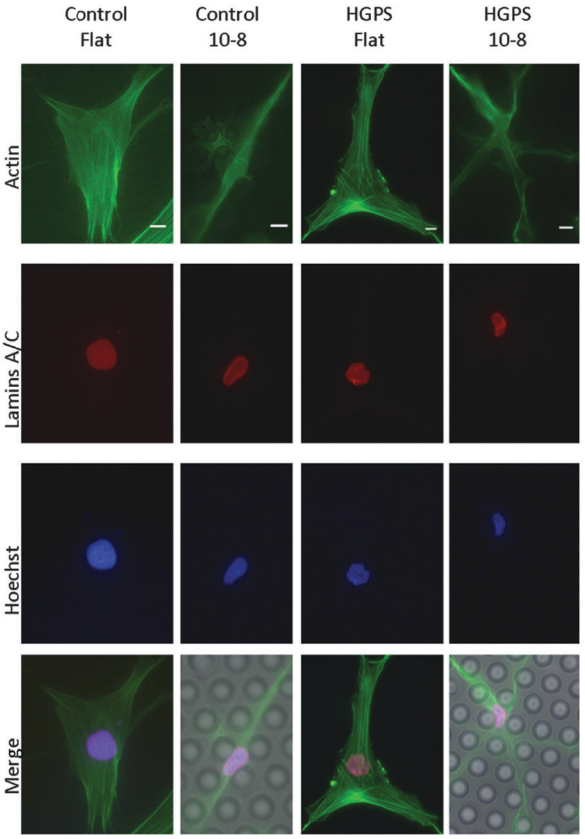

Fig. 2 Actin and lamin structures adapt to μP environment. HGPS and control cells with labelled actin (Oregon Green Phallodin), lamin A/C (immunostained with Alexa Fluor 555) and DNA (Hoechst 33342) on flat substrates and in 10-8 substrates. The control nuclei were consistently smooth on both substrates. The HGPS nuclei showed blebbing and invaginations on the flat substrate and additionally show creasing on the 10-8 substrate. Both cell types show characteristic branching of the actin cytoskeleton in the μP array. Scale bars are 10 μm.

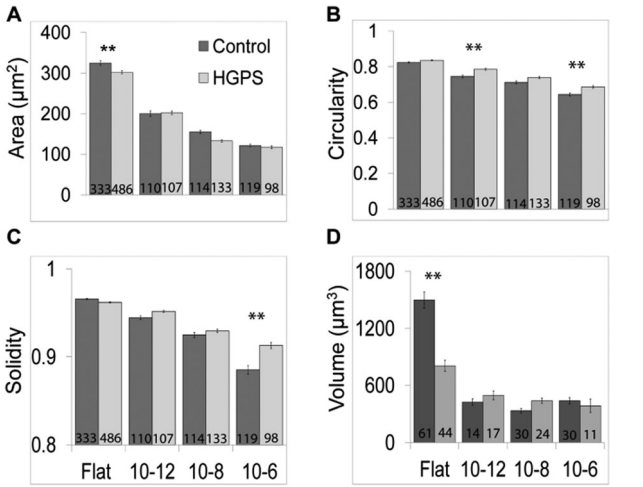

Fig. 3 Morphometric analysis of nuclei in varied micropillar spacings. Analysis of the area (A), circularity (B), solidity (C), and volume (D) of the HGPS and control cells on substrates with various pillar spacing. Numbers at the bottom of bar graphs are cells used in analysis. Increases in circularity and solidity suggest that HGPS cells are less able to deform their nuclei in the μPs. Error bars are SEM and $^{**}p < 0.01$.

showed a cross sectional nuclear area similar to or slightly larger than that of the HGPS cells at nearly all μP geometries tested (Fig. 3A). The increased projected area of control cells[16] may reflect easier nuclear deformability and recovery within changing environments. Cross sectional area of HGPS cells in 10-6 spacing showed a 63% decrease in cross sectional area while the control cells showed a 70% decrease in cross sectional area (Fig. 3A). HGPS nuclei showed an increased stiffening of the nucleoskeleton and a concentration of lamin proteins at the nuclear periphery in 2D cultures.[17] HGPS nuclei, showed dysmorphic microstructures (Fig. 1), but also showed a more circular overall shape compared with control cells (higher circularity, Fig. 3) since the micro-dysmorphic shapes prevented proper elongation of nuclei.[29] Circularity, which quantified both elongation and blebs, was greater for HGPS nuclei than control nuclei at every condition tested (Fig. 3B). The 10-6 spacing compared to flat substrates showed a decrease in circularity values of 18% for HGPS nuclei and 22% for control nuclei. We used solidity as a parameter to quantify gross concavity of nuclei. Solidity is the ratio of the nuclear area over the area of the convex hull, thus decreases in solidity are associated with nuclei that are able to deform around the micropillar substrates. It appeared that solidity decreased more for control nuclei as μP spacing decreased than for HGPS nuclei (Fig. 3C). The 10-6 spacing showed a decrease of 5.0% for HGPS nuclei and 8.4% for control nuclei. This again suggested that the control nuclei were better able to conform to the restricted contours of the μP array.

Nuclei were also imaged in 3D by taking *z* series of cells in micropillars and on flat substrates (see Methods). The volume of the HGPS nuclei on flat substrates was found to be significantly smaller than the volume of the control cell nuclei (Fig. 3D). When the nuclei entered the 3D μP structures there was a significant decrease in the nuclear volume for both the HGPS and control cells. Additionally, any difference in nuclear volume between the control and HGPS cells as seen on a 2D substrate was no longer present in the 3D μP environment regardless of spacing. Additionally, there was no difference in the volume of the nuclei in the micropillars regardless of spacing for HGPS and control cells. The ~70% decrease in volume for the control cells and the ~50% decrease in volume for the HGPS cells when entering the micropillars suggest that the nuclei deform and compress to accommodate cell invasion. A ~70% decrease in nuclear volume is consistent with results seen during micropipette aspiration studies[30] and over the course of the cell cycle.[31]

Cell migration and spacing in ECM

To study invasion and transmigration of HGPS and control fibroblasts, we quantified the cell's ability to enter the μP arrays and movement within the μPs, respectively. Control NIH-3T3 fibroblasts showed a decreased ability to enter the μP array with reduced inter-μP spacing (Fig. 4A). Fewer primary fibroblasts from HGPS patients were able to enter the μP array compared with the control cells at all spacings (Fig. 4B). Some cells

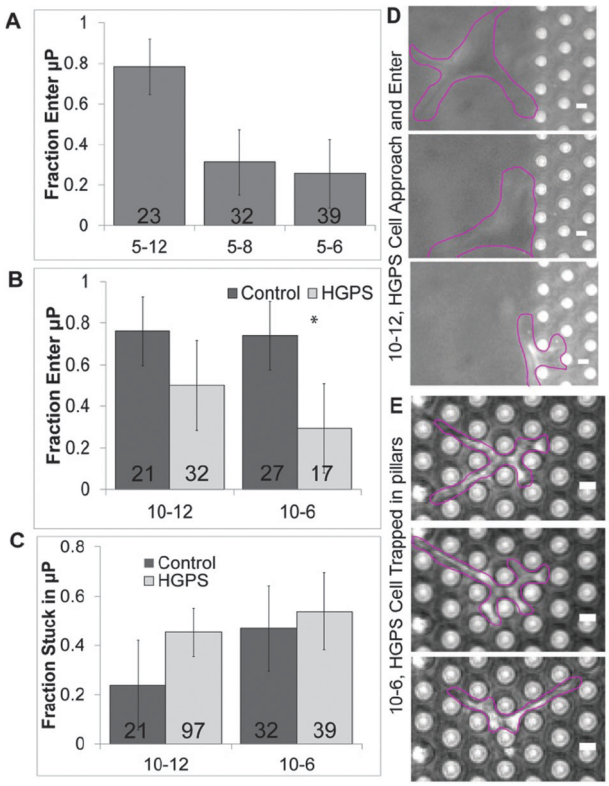

Fig. 4 Characterizing ability of HGPS and control cells to enter and transmigrate through micropillars. (A) Proportion of NIH 3T3 cells that were able to enter the µPs from the flat substrate over 24 hours, with varied pillar spacing. (B) Proportion of HGPS and control cells that were able to invade the µPs from the flat substrate over 24 hours, with varied pillar spacing. Fisher exact test was used to determine significance at $p < 0.05$ (*). (C) Proportion of cells in the µPs that remained stuck in a single location over a 24 h imaging period. (A–C) error bars are 95% confidence intervals. (D) Example of a cell entering the µPs, 10-12. (E) Example of a cell remaining at a single location in the µPs over 24 hours, 10-6. Numbers at the bottom of bar graphs are count of cells used in analysis. Magenta outlines of cells are provided to guide the readers eye to cell locations. Scale bars are 10 µm.

became lodged in the µP array and were unable to move for the duration of the imaging (24 hours). Inside the pillars, HGPS fibroblasts were often stuck suggesting an inability to transmigrate within the µP array (Fig. 4C). When the HGPS cells were stuck in the µP array, cells extended protrusions (*e.g.* Fig. 2, HGPS 10-8), which were observed with live cell imaging. We suggest that HGPS cells become stuck from stiffened nuclei and compensate by creating cytoskeletal protrusions to generate force to dislodge themselves.[22]

Although some cells became stuck in the µP array, many of the cells were able to migrate through the µPs. Cell migration through the µP array fit to a persistent random walk equation (see Methods, Fig. 5B. Movie S1 and S2, ESI†).[32] At short time scales (less than 400 minutes) cells showed a persistent directed motion. At long time scales cells showed a diffusive motion consistent with previous data.[22] Due to their decreased migration the HGPS cells showed the beginning of the diffusive response at shorter time scales when in µPs, on the order of tens of minutes. Example trajectories of control fibroblasts (Fig. 5A) show higher motility and increased distance of migration compared with the HGPS cells (Fig. 5B). Mean square displacement (MSD) of the movement of the control and HGPS cells highlights the differences between the cell populations. Control and HGPS cell nuclei show similar mean square displacement (MSD) profiles on flat substrates (Fig. 5C), suggesting that HGPS and control cells have similar motility. The 3D µP environment greatly altered HGPS cells motility, with a >70% decrease from flat substrates to 12 µm µP spacing; control cells showed an <20% decrease in the diffusion coefficient under the same conditions (Fig. 5C and D). Although HGPS cells showed a dramatic decrease in motility from flat surfaces to the µP array, there was only a 4.44% difference in different pillar spacing (Fig. 5C). Control cells were more affected by this µP spacing (Fig. 5C), and cells showed a steady decrease in MSD *versus* time with decreased pillar spacing (Fig. 5D).

Progerin disrupts force generation across the cell

Altered diffusion in any system is both a function of resistance to movement and driving force. As such, we considered the possibility of altered force generation by HGPS cells. To measure cellular force generation on extracellular materials, we used traction force microscopy of patterned cells on deformable substrates (Fig. 6 and Methods). HGPS cells showed a 61% decrease in cell traction force compared to the control fibroblasts (Fig. 6B, D and E). Despite uniform pattern size, HGPS cells had a higher projected area on the polyacrylamide substrate (Fig. 6C and F) as a consequence of reduced inward force generation (Fig. 6D). The reduced inward force suggests that HGPS alters normal force propagation within the cell and may have implication in cell mobility. The overall force generation of control cells was 1.6 times that of HGPS cells, and the maximum traction force generated by the control cells was 2.5 times greater than the maximum traction force generated by the HGPS cells.

Spatial imaging of force generation from control cells from the center of the cell to the edge showed an observable spatial increase in force generation at ~10 µm from the center (Fig. 6F), consistent with the edge of the nucleus in control cells. HGPS cells showed no such transition as well as an overall reduction in traction force (Fig. 6F). The consistent overall decrease in traction force generated within HGPS and between HGPS cells and the extracellular environment could partially explain the HGPS cells decreased ability to invade and transmigrate within the µP array.

Discussion

Native ECM provides cells with many chemical, mechanical, spatial, topographical and temporal cues to influence cell behavior including pores for cell induction and migration, which can range from tens of nanometers to hundreds of micrometers.[33] Cell invasion requires translocation in multidimensional environments with different chemical and mechanical properties. Cell migration through ECM is necessary for

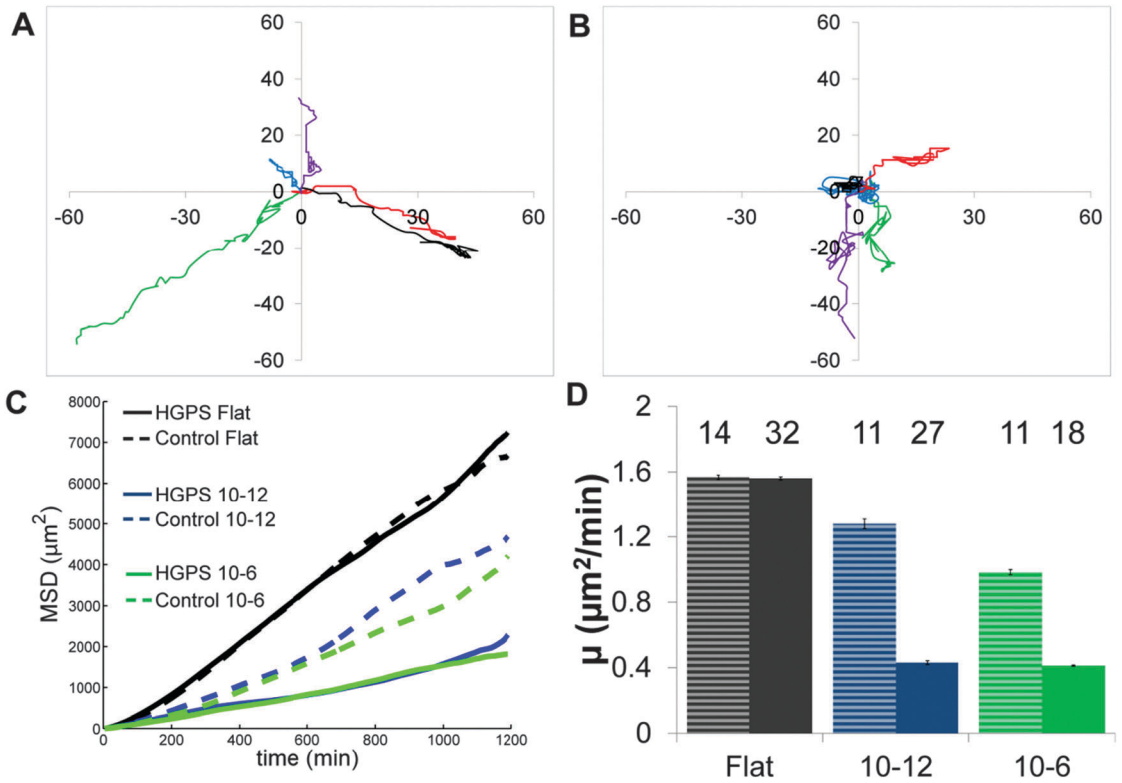

Fig. 5 Quantitative analysis of cellular migration of HGPS and control fibroblasts through μPs. Example trajectories from (A) control cells and (B) HGPS cells in 10-6 μPs over 360 minutes. (C) Plot of MSD as a function of time for control and HGPS cells shows no differences in cell speed on flat substrates (black lines). Control cells (dashed lines) within the μP arrays showed reduced motility from a flat substrate. The speed of HGPS cells (solid lines) is more substantially impacted by movement through the μP array. (D) Comparison of random walk diffusion coefficients, *μ*, highlight the reduced motility of HGPS cells (solid) within the μPs compared with control (stripes). Number of cells used for analysis in C and D are shown above the bar. Error bars are 95% confidence intervals of the diffusion coefficient.

development, wound healing, invasion of cells into artificial biomaterials; cancer metastasis also requires cellular invasion into and migration through interstitial spaces. Most invasion and transmigration studies focus on focal adhesions,[22,24,33] cytoskeletal structures and force generation,[7,8,34] which are critical to these processes. There have been few studies of mechanically-resistive elements in transmigration and invasion.[4] The nucleus is shown to be increasingly important in pathological cell migration including cancer metastasis[35] and we suggest that a stiffened nucleus may reduce wound healing in advanced aging.

Measuring cell migration with PDMS pillars

In this study, precisely-spaced μPs were used to provide the cell with a homogenous, non-degradable, 3D microenvironment with tunable spacing. The use of these uniform substrates allowed monitoring of nuclear deformation in a controlled environment without cell induced substrate changes. We showed that the stiffness of the nucleus is crucial in cell invasion and transmigration. Small inter-pillar spacing correlated with increased nuclear deformation upon entry into microfabricated substrates and decreased transmigration within the substrates. When entering the substrates the projected area of the nucleus, circularity, and solidity decrease. These factors are also reduced with pillar spacing suggesting nuclear changes during movement from a 2D to a 3D environment.[22] Decreased μP spacing inhibited cellular entry into the μP array, particularly for HGPS cells, motility decreased with decreasing pillar spacing. Nuclei showed defects as a function of pillar spacing, suggesting an inverse relationship between nuclear morphology and cell motility. When the nucleus and nucleoskeleton were able to smoothly deform, as seen at higher μP spacing, the cell was able to smoothly migrate between the μPs. However, when mechanical discontinuities developed from defects in the nucleoskeleton in tight μP spacing, the cells had difficulty migrating. Thus, the stiffer HGPS nucleoskeleton[16] reduced overall cell motility.

Cellular aging in Hutchinson–Gilford progeria syndrome

Hutchinson–Gilford progeria syndrome results from a single *de novo* point mutation in the *LMNA* gene resulting in the activation of a cryptic splice site, the loss of 50 amino acids, and incorrect downstream protein processing.[13] Progerin, the lamin A mutant, maintains a farnesyl group and is anchored to the inner nuclear membrane.[36] This results in the formation of progerin-based micro-aggregates in the nucleoskeleton and a stiffening of the nucleoskeleton.[16] The HGPS patient cells studied here were from an 8.5 year old male with the C > T mutation in exon 11 in *LMNA*, which is responsible for ~80% of

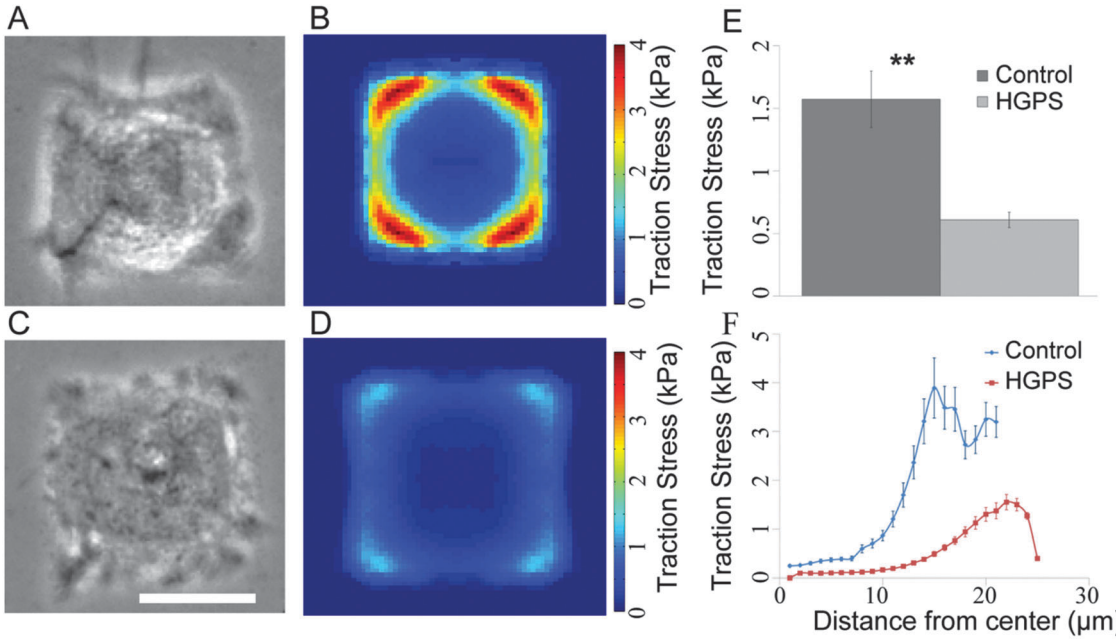

Fig. 6 HGPS cells show decreased traction force. Phase contrast and corresponding traction force stress maps of control (A, B) and HGPS fibroblasts (C, D) on patterned polyacrylamide gels embedded with fluorescent particles (see Methods). (E) Comparison of average traction force of control and HGPS cells (n = 16, each). (F) Trace of traction for extending outward from cell center to cell corner. Control cells showed a transition in stress at 10 μm. HGPS cells showed no transition and a consistent decrease in traction force measurements across trace. Error bars are SEM. $^{**}p < 0.01$. Scale bar is 25 μm.

the reported HGPS cases.[37] The activation of this cryptic splicing also occur sporadically in healthy patients, and progerin accumulates in healthy nuclei over decades.[20,38,39] Thus, studying the migration of progerin-stiffened nuclei is important in the etiology of HGPS as well as for understanding how cell migration changes during normal aging.

The LINC complex provides a direct physical connection between the cytoskeleton and the nucleoskeleton. In progeriod mouse models both nucleoskeletal and cytoskeletal mechanics are altered, suggesting a breakdown in LINC connections.[40] Progerin alters levels and localization of LINC proteins.[41] The breakdown in nucleoskeletal–cytoskeletal connections could contribute to decreased traction force and cell motility. When migrating through the nuclear-restricting environment, the HGPS cells move more slowly than control cells likely from a combination of increased nuclear stiffness and decreased traction force. We have shown here that exogenous expression of progerin causes significant changes in cellular motility through 3D environments.

Aging causes stiffening of the ECM from increased cross-linking of the collagen matrix through glycosylation, by-products of lipid oxidation, and exposure to UV light. Here, the stiffness of the PDMS substrates was not modulated but smaller inter-pillar spacing could mimic altered ECM structure. Cells will move rapidly through matrices where the pore size is similar to the cell size minimizing the need for cell deformation and proteolytic cleavage, but at decreasing spacing the need for cell deformation increases and migration slows. HGPS cells were less able to enter tight μP arrays and showed decreased motility in pillared substrates. Additionally, there was a minimal difference in the motility coefficient of the HGPS cells in the μP array regardless of spacing. The decreased motility upon entry into the substrates suggests that with increased stiffness in the nuclei compounded by decreased traction force it has become difficult enough for the cells to migrate through the 3D substrate such that decreased spacing has minimal impact. The ECM can have very small pore sizes that would inhibit or slow cell migration, making the cells more dependent on processes such as proteolysis during migration. This is in contrast to the control cells where there is a gradual decline in cell movement inside μP array with decreased spacing. Thus, we suggest that progeriod and potential aged cells have reduced ability to crawl in 3D matrices. This could reduce the potential for wound healing, integration of cells into biomaterial devices, and, possibly cell migration with cancer. With aging, cancer is a large risk factor with the accumulation of mutations over a lifetime.[42] The increased stiffness of the ECM in older patients could work to reduce the metastatic potential of cancer in an aged population.

In this work we showed that uniform changes in spacing of the cell microenvironment resulted in changes in nuclear morphology and in decreased ability of cells to migrate through the substrates. When the nucleus was stiffened as modeled by HGPS there was already increased dysmorphic nuclei, changes in nuclear morphology, stiffening the nucleus, and decreases in traction force caused a dramatic drop in diffusion coefficient for migration through the micropillar substrate regardless of the spacing. This suggests that not only does the ECM stiffen during the aging process but the additional stiffening of the nucleus compounds the problem, further decreasing the cells ability to migrate.

Materials and methods

Cell culture and transfection

NIH 3T3 with endogenous lamin A GFP[43] were cultured in Dulbecco's modified Eagle medium (DMEM) containing 10% fetal bovine serum and 1% penicillin/streptomycin (all from Invitrogen, Carlsbad, CA). Central Dogma (CD) tagging was used to create NIH 3T3 cell lines with a naturally regulated GFP lamin A in the genome.[43] Fibroblasts were generously donated from the Progeria Research Foundation (Peabody, MA) and were cultured in DMEM with high glucose, 15% fetal bovine serum, 1% L-glutamine and 1% penicillin/streptomycin (Invitrogen, Carlsbad, CA). Two cells lines from the Progeria Research Foundation were used: an HGPS cell line (HGADFN167, referred to as HGPS) with the mutation CT608 in exon 11, and an adult control (HGADFN168, referred to as control) from a 40 year parent, negative for the point mutation. The HGPS and control fibroblasts were used between passage 29 and 33, adequately late passage to show the nuclear defects associated with HGPS.

Fabrication of polydimethylsiloxane substrates

Polydimethylsiloxane (PDMS, Sylgard 184, Dow Corning, Midland, MI) micropillar array were prepared according to previous studies.[26] Briefly, PDMS was poured over silicium wafer, cured at 65 °C for 15 ± 2 h and peeled off the wafer in dry conditions. PDMS substrates were plasma treated (Harrick Plasma Cleaner and Sterilizer PDC-32G, Ithaca, NY) in preparation for fibronectin adhesion. PDMS substrates consisted of regions of flat surface bordered by region of μP array, as seen in Fig. 4. To coat PDMS substrates with fibronectin, 200 μL of 10 μg mL^{-1} was added directly to the substrate and incubated on bench top (Sigma-Aldrich, Saint-Quentin Fallavier, France, or St. Louis, MO) in phosphate buffered saline for 1 h, coating both the flat and μP regions of the substrate in fibronectin. Cells were then seeded on the PDMS substrate at 20% confluency and incubated at cell culture conditions for 7 hours prior to imaging.

Immunofluorescent staining and morphological analysis

After 30 ± 3 hours on the various substrates, F-actin and lamins A/C were imaged. Cells were fixed with 3.7% formaldehyde in PBS, permeabilized with 0.1% Triton X-100 in PBS and blocked with 0.2% bovine serum albumin (BSA; Sigma-Aldrich, St. Louis, MO). F-actin was labelled with Oregon green phallodin (2.5 : 100 dilution; O7466, Invitrogen, Carlsbad, CA). Lamin A/C was labelled by rabbit polyclonal antibody (1 : 100 sc-7293 Santa Cruz Biotechnology, Santa Cruz, CA). Alexa Fluor goat anti-rabbit 555 (1 : 200 catalog number, Invitrogen, Carlsbad, CA). DAPI (1 : 4000 of 1 mg mL^{-1}; Invitrogen, Carlsbad, CA) was added to label DNA. Images were taken on a Leica DMI6000B inverted microscope with A, I3, and N2.1 filter cubes (Leica, Buffalo Grove, IL).

ImageJ (National Institutes of Health, Bethesda, MD) was used to analyze the lamin A/C channel of the immunofluorescent images. Between 98 and 140 cell nuclei were analysed for each data set. Nuclei were analysed for changes in area, circularity, solidity, and dysmorphic nuclei were counted. Circularity was defined in eqn (1) where A is the area and P is the perimeter. While circularity gives a measure of how the perimeter of the structure departs from that of a smooth circle, solidity provides a sense of the irregularity of the object.

$$\text{Circularity} = 4\pi A/P^2 \quad (1)$$

$$\text{Solidity} = \text{area/convex area} \quad (2)$$

Nikon C2 laser scanning confocal microscope (Nikon, Melville, NY) with a three channel fluorescence detectors was used to take 3D stacks of cells in μPs. The cells were stained as before with Oregon green phallodin, DAPI, and lamin A/C was labelled by mouse polyclonal antibody (1 : 100 sc-7292, Santa Cruz Biotechnology, Santa Cruz, CA). Alexa fluor donkey anti-mouse 594 (1 : 200 A21203, Invitrogen, Carlsbad, CA). 3D volumetric analysis was done using ImageJ plugin 3D object counter. The voxel information provided was scaled to provide nuclear volume information. Dysmorphic nuclei showed blebbing, invagination, or creasing and a normal nucleus appeared ovoid or smoothly deformed by the micropillars. Statistical comparisons of area, circularity, solidity, and volume were determined by two way ANOVA test with a Bonferroni correction for multiple comparisons. Fisher's exact test was used to compare counts of dysmorphic cells.

Time lapse video microscopy

We acquired time-lapse images of cells on pillars on an Olympus IX71 inverted microscope (Olympus, Rungis, France), and a Leica DMI6000B (Leica, Buffalo Grove, IL). Both microscopes were equipped with heaters to maintain a temperature of 37 °C. Cell media was changed 2 hours prior to the experiment to leibovitz media which does not require 5% CO_2 (Invitrogen, Carlsbad, CA). To prevent evaporation, a layer of mineral oil (Sigma-Aldrich, St. Louis, MO) was floated on top of the media prior to imaging. Images were acquired every 5 minutes. A Photometrics Coolsnap ES (Olympus inverted microscope, Roper Scientific, Evry, France), HQ2 (Olympus upright microscope, Roper Scientific, Evry, France), and Leica DFC350 (Leica, Buffalo Grove, IL) cameras were used. The Olympus microscopes used Metamorph software (Universal Imaging Corporation, Downingtown, PA) and the Leica microscope used Leica software (Leica, Buffalo Grove, IL).

For the trajectory experiments images were acquired every 5 minutes for 24 hours on the inverted Olympus microscope using an Olympus 20× air objective (NA 0.40) or on the Leica microscope using a Leica 20× air objective (NA 0.40). The Olympus microscope used a motorized stage (Marzhauser, Wetzler, Germany) and the Leica used a Leica motorized stage (Leica, Buffalo Grove, IL). Between 12 and 20 positions were imaged in a 24 hour period. Prior work[22] compared 5 and 10 μm pillar heights showed a transition from crawling on top of the μPs (5 μm) to crawling within the μPs (10 μm), with this in mind we increased the height to 20 μm to ensure that many of the cells migrated through the μPs. Some cells may have migrated over the tops of the μPs, but these cells were not

visible in the focal plane used during image capture and were thus excluded from analysis.

Quantitative analysis of individual cell motility

To quantify cell migration, we analysed the time-lapse images with ImageJ (NIH, Bethesda, MD) plugins. First, microscope vibration was removed with the image stabilizer plugin (Li 2008). Cells undergoing division or blebbing were removed from analysis. Non-motile cells were defined as cells that did not move more than 10 μm or past one μP in 24 hours. Due to the light refraction off the 20 μm tall pillars, automated image analysis was not consistently possible and manual tracking was employed using the Manual Tracking ImageJ plugin. By knowing all the positions as a function of time, mean squared displacement could be determined. For each substrate MSD curves were fitted to 20 hours of data for 18–32 different cells, corresponding to cell tracking for at least 18 hours (1100 min). Raw data and fitting for all times is available in ESI.†

$$\langle r^2(\tau)\rangle = \langle [x(t+\tau) - x(t)]^2 + [y(t+\tau) - y(t)]^2\rangle \quad (3)$$

At long times the MSD of the cell migration showed a time dependant increase such that

$$\langle r^2(\tau)\rangle = \mathrm{MSD}(\tau) \approx \tau^{\beta} \quad (4)$$

The persistent random walk equation was then used to fit the MSD data.

$$\langle r^2(\tau)\rangle = 2n_d\mu[\tau - P(1 - e^{((-\tau)/P)})] \quad (5)$$

P is the directional persistence time, μ is the diffusion coefficient which is analogous to a molecular diffusion coefficient, and n_d is the number of dimensions.[32]

Traction force microscopy

Traction force microscopy measurements were done as previously published in Rape *et al.*[44] Briefly, a positive photoresist, SPR-220.3 (Microchem, Newton, MA) was spun on a glass coverslip. It was exposed to UV light through a patterned photomask and developed as molding for PDMS (Dow Corning, Midland, MI).[45] PDMS pre-polymers were mixed with catalyst and poured over the coverslip and cured at 60 °C for 1 hour. The PDMS stamp was then cut away and incubated with activated gelatin solution for 30 minutes after which excess gelatin was blown away with a Nitrogen stream. Polyacrylamide was prepared with 5% acrylamide (BioRad, Hecules, CA), 0.1% bisarcylamide (BioRad) and 1 : 1000 dilution of 0.2 μm fluorescent latex beads (Molecular Probes, Carlesbad, CA). 30 μL of the solution with initiators was pipetted onto a large Bind-Silane (GE Healthcare, Waukesha, WI) activated coverslip. The stamp was place patterned side down onto the acrylamide solution and after polymerization the top coverslip was gently removed. Cells were seeded overnight on an array of 50 × 50 μm squares that were functionalized and only cells that adhered to the entire a square region (50 × 50 μm) were considered for analysis. Images were collected on an Axiovert S100TV (Carl Zeiss, Thornwood, NY) microscope equipped with a 40× plan neofluor air objective. A fluorescent image of the beads near the ventral surface of the cells was collected. The cells were trypsinized and released. A second fluorescent image of the beads in the relaxed position was acquired. Substrate displacement fields and the corresponding traction stress maps were computed using custom software and the LIBTRC package (courtesy of Dr Micah Dembo, Boston University).[45]

Author contributions

EBG, KND, BL and MG designed and initiated the study. VD, MG performed NIH3T3 cell tracking experiments and analysis. EBG performed HGPS fibroblast and control tracking experiments and analysis. AR performed traction force microscopy studies. EBG, KND, and BL wrote the manuscript.

Acknowledgements

The authors would like to thank I. Motta, L. Trichet for critical discussions and tracking experiments of NIH 3T3. We thank the Progeria Research Foundation for cells from HGPS patients and J. Jarvik (Carnegie Mellon Biology) for 3T3 cells with endogenous GFP lamin A expression, A. Richert for cell culture protocols and A. Riberio for his helpful discussions. We acknowledge support from NSF CBET (0954421) and Progeria Research Foundation (to KND) and Financial support from the Association pour la Recherche sur le Cancer (ARC), the Association Française contre la Myopathie (AFM) and the Agence Nationale de la Recherche (ANR 2010 BLAN 1515 MECANOCAD; ANR Blanc Inter SVSE 5 2010 NMVASC) (to BL) are gratefully acknowledged. The research was conducted in the scope of the International Associated Laboratory Cell Adhesion France-Singapore (LIA CAFS).

Notes and references

1 B. A. Harley, H. D. Kim, M. H. Zaman, I. V. Yannas, D. A. Lauffenburger and L. J. Gibson, *Biophys. J.*, 2008, **95**, 4013–4024.
2 S. Schmidt and P. Friedl, *Cell Tissue Res.*, 2010, **339**, 83–92.
3 P. Friedl and K. Wolf, *Cancer Metastasis Rev.*, 2009, **28**, 129–135.
4 P. Friedl, K. Wolf and J. Lammerding, *Curr. Opin. Cell Biol.*, 2011, **23**, 55–64.
5 K. Wolf, I. Mazo, H. Leung, K. Engelke, U. H. von Andrian, E. I. Deryugina, A. Y. Strongin, E. B. Brocker and P. Friedl, *J. Cell Biol.*, 2003, **160**, 267–277.
6 M. H. Zaman, L. M. Trapani, A. L. Sieminski, D. Mackellar, H. Gong, R. D. Kamm, A. Wells, D. A. Lauffenburger and P. Matsudaira, *Proc. Natl. Acad. Sci. U. S. A.*, 2006, **103**, 10889–10894.
7 W. R. Legant, J. S. Miller, B. L. Blakely, D. M. Cohen, G. M. Genin and C. S. Chen, *Nat. Methods*, 2010, **7**, 969–971.
8 M. Ghibaudo, J. M. Di Meglio, P. Hersen and B. Ladoux, *Lab Chip*, 2011, **11**, 805–812.
9 K. N. Dahl, E. A. Booth-Gauthier and B. Ladoux, *J. Biomech.*, 2010, **43**, 2–8.

10 K. J. Roux, M. L. Crisp, Q. Liu, D. Kim, S. Kozlov, C. L. Stewart and B. Burke, *Proc. Natl. Acad. Sci. U. S. A.*, 2009, **106**, 2194–2199.
11 A. Mazumder and G. V. Shivashankar, *J. R. Soc., Interface*, 2010, **7**(suppl 3), S321–S330.
12 K. N. Dahl and A. Kalinowski, *J. Cell Sci.*, 2011, **124**, 675–678.
13 M. Eriksson, W. T. Brown, L. B. Gordon, M. W. Glynn, J. Singer, L. Scott, M. R. Erdos, C. M. Robbins, T. Y. Moses, P. Berglund, A. Dutra, E. Pak, S. Durkin, A. B. Csoka, M. Boehnke, T. W. Glover and F. S. Collins, *Nature*, 2003, **423**, 293–298.
14 R. D. Goldman, D. K. Shumaker, M. R. Erdos, M. Eriksson, A. E. Goldman, L. B. Gordon, Y. Gruenbaum, S. Khuon, M. Mendez, R. Varga and F. S. Collins, *Proc. Natl. Acad. Sci. U. S. A.*, 2004, **101**, 8963–8968.
15 D. K. Shumaker, T. Dechat, A. Kohlmaier, S. A. Adam, M. R. Bozovsky, M. R. Erdos, M. Eriksson, A. E. Goldman, S. Khuon, F. S. Collins, T. Jenuwein and R. D. Goldman, *Proc. Natl. Acad. Sci. U. S. A.*, 2006, **103**, 8703–8708.
16 K. N. Dahl, P. Scaffidi, M. F. Islam, A. G. Yodh, K. L. Wilson and T. Misteli, *Proc. Natl. Acad. Sci. U. S. A.*, 2006, **103**, 10271–10276.
17 J. T. Philip and K. N. Dahl, *J. Biomech.*, 2008, **41**, 3164–3170.
18 P. Scaffidi and T. Misteli, *Science*, 2006, **312**, 1059–1063.
19 E. Haithcock, Y. Dayani, E. Neufeld, A. J. Zahand, N. Feinstein, A. Mattout, Y. Gruenbaum and J. Liu, *Proc. Natl. Acad. Sci. U. S. A.*, 2005, **102**, 16690–16695.
20 P. Scaffidi, L. Gordon and T. Misteli, *PLoS Biol.*, 2005, **3**, e395.
21 T. Aigner, J. Haag, J. Martin and J. Buckwalter, *Curr. Drug Targets*, 2007, **8**, 325–331.
22 M. Ghibaudo, L. Trichet, J. Le Digabel, A. Richert, P. Hersen and B. Ladoux, *Biophys. J.*, 2009, **97**, 357–368.
23 J. D. Pajerowski, K. N. Dahl, F. L. Zhong, P. J. Sammak and D. E. Discher, *Proc. Natl. Acad. Sci. U. S. A.*, 2007, **104**, 15619–15624.
24 M. T. Frey, I. Y. Tsai, T. P. Russell, S. K. Hanks and Y. L. Wang, *Biophys. J.*, 2006, **90**, 3774–3782.
25 J. L. Tan, J. Tien, D. M. Pirone, D. S. Gray, K. Bhadriraju and C. S. Chen, *Proc. Natl. Acad. Sci. U. S. A.*, 2003, **100**, 1484–1489.
26 O. du Roure, A. Saez, A. Buguin, R. H. Austin, P. Chavrier, P. Silberzan and B. Ladoux, *Proc. Natl. Acad. Sci. U. S. A.*, 2005, **102**, 2390–2395.
27 P. Clark, P. Connolly, A. S. Curtis, J. A. Dow and C. D. Wilkinson, *Development*, 1987, **99**, 439–448.
28 B. C. Capell, M. R. Erdos, J. P. Madigan, J. J. Fiordalisi, R. Varga, K. N. Conneely, L. B. Gordon, C. J. Der, A. D. Cox and F. S. Collins, *Proc. Natl. Acad. Sci. U. S. A.*, 2005, **102**, 12879–12884.
29 S. Choi, W. Wang, A. J. Ribeiro, A. Kalinowski, S. Q. Gregg, P. L. Opresko, L. J. Niedernhofer, G. K. Rohde and K. N. Dahl, *Nucleus*, 2011, **2**, 570–579.
30 A. C. Rowat, J. Lammerding and J. H. Ipsen, *Biophys. J.*, 2006, **91**, 4649–4664.
31 P. Roca-Cusachs, J. Alcaraz, R. Sunyer, J. Samitier, R. Farre and D. Navajas, *Biophys. J.*, 2008, **94**, 4984–4995.
32 R. B. Dickinson and R. T. Tranquillo, *AIChE J.*, 1993, **39**, 1995–2010.
33 E. Cukierman, R. Pankov and K. M. Yamada, *Curr. Opin. Cell Biol.*, 2002, **14**, 633–639.
34 K. Wolf and P. Friedl, *Clin. Exp. Metastasis*, 2009, **26**, 289–298.
35 J. Brabek, C. T. Mierke, D. Rosel, P. Vesely and B. Fabry, *Cell Commun. Signaling*, 2010, **8**, 22.
36 M. W. Glynn and T. W. Glover, *Hum. Mol. Genet.*, 2005, **14**, 2959–2969.
37 D. McClintock, L. B. Gordon and K. Djabali, *Proc. Natl. Acad. Sci. U. S. A.*, 2006, **103**, 2154–2159.
38 D. McClintock, D. Ratner, M. Lokuge, D. M. Owens, L. B. Gordon, F. S. Collins and K. Djabali, *PLoS One*, 2007, **2**, e1269.
39 K. Cao, C. D. Blair, D. A. Faddah, J. E. Kieckhaefer, M. Olive, M. R. Erdos, E. G. Nabel and F. S. Collins, *J. Clin. Invest.*, 2011, **121**, 2833–2844.
40 C. M. Hale, A. L. Shrestha, S. B. Khatau, P. J. Stewart-Hutchinson, L. Hernandez, C. L. Stewart, D. Hodzic and D. Wirtz, *Biophys. J.*, 2008, **95**, 5462–5475.
41 F. Haque, D. Mazzeo, J. T. Patel, D. T. Smallwood, J. A. Ellis, C. M. Shanahan and S. Shackleton, *J. Biol. Chem.*, 2010, **285**, 3487–3498.
42 A. Marusyk and J. DeGregori, *Biochim. Biophys. Acta*, 2008, **1785**, 1–11.
43 J. W. Jarvik, G. W. Fisher, C. Shi, L. Hennen, C. Hauser, S. Adler and P. B. Berget, *Biotechniques*, 2002, **33**, 852–4, 856, 858–60 passim.
44 A. D. Rape, W. H. Guo and Y. L. Wang, *Biomaterials*, 2011, **32**, 2043–2051.
45 M. Dembo and Y. L. Wang, *Biophys. J.*, 1999, **76**, 2307–2316.